BBA - Molecular Basis of Disease 1865 (2019) 434–444

Contents lists available at ScienceDirect

BBA - Molecular Basis of Disease

journal homepage: www.elsevier.com/locate/bbadis

Nucleation of β-rich oligomers and β-barrels in the early aggregation of human islet amyloid polypeptide

Yunxiang Sun[a], Aleksandr Kakinen[b], Yanting Xing[a], Emily H. Pilkington[b,c], Thomas P. Davis[b,c], Pu Chun Ke[b,*], Feng Ding[a,*]

[a] Department of Physics and Astronomy, Clemson University, Clemson, SC 29634, USA
[b] ARC Centre of Excellence in Convergent Bio-Nano Science and Technology, Monash Institute of Pharmaceutical Sciences, Monash University, 381 Royal Parade, Parkville, VIC 3052, Australia
[c] Department of Chemistry, University of Warwick, Coventry CV4 7AL, UK

ARTICLE INFO

Keywords:
Type 2 diabetes
Amyloid aggregation
Oligomerization
β-Barrel oligomer
Nucleation
Discrete molecular dynamics simulations

ABSTRACT

The self-assembly of human islet amyloid polypeptide (hIAPP) into β-sheet rich amyloid aggregates is associated with pancreatic β-cell death in type 2 diabetes (T2D). Prior experimental studies of hIAPP aggregation reported the early accumulation of α-helical intermediates before the rapid conversion into β-sheet rich amyloid fibrils, as also corroborated by our experimental characterizations with transmission electron microscopy and Fourier transform infrared spectroscopy. Although increasing evidence suggests that small oligomers populating early hIAPP aggregation play crucial roles in cytotoxicity, structures of these oligomer intermediates and their conformational conversions remain unknown, hindering our understanding of T2D disease mechanism and therapeutic design targeting these early aggregation species. We further applied large-scale discrete molecule dynamics simulations to investigate the oligomerization of full-length hIAPP, employing multiple molecular systems of increasing number of peptides. We found that the oligomerization process was dynamic, involving frequent inter-oligomeric exchanges. On average, oligomers had more α-helices than β-sheets, consistent with ensemble-based experimental measurements. However, in ~4–6% independent simulations, β-rich oligomers expected as the fibrillization intermediates were observed, especially in the pentamer and hexamer simulations. These β-rich oligomers could adopt β-barrel conformations, recently postulated to be the toxic oligomer species but only observed computationally in the aggregates of short amyloid protein fragments. Free-energy analysis revealed high energies of these β-rich oligomers, supporting the nucleated conformational changes of oligomers in amyloid aggregation. β-barrel oligomers of full-length hIAPP with well-defined three-dimensional structures may play an important pathological role in T2D etiology and may be a therapeutic target for the disease.

1. Introduction

Aberrant aggregation of human islet amyloid polypeptide (hIAPP) into insoluble amyloid fibrils is a hallmark of type 2 diabetes (T2D) [1]. Similarly to other amyloid proteins such as amyloid-β (Aβ) [2], associated with Alzheimer's disease, and α-synuclein [3] in Parkinson's disease, the amyloid fibrils of hIAPP display the characteristic “cross-β” core structures [4–6]. Experimentally-observed sigmoidal kinetics reveals a nucleation process of amyloid aggregation, where the initial lag phase corresponds to the assembly of soluble oligomers and nucleation of β-rich aggregates before their rapid elongation/growth into protofibrils and saturation of mature fibrils [7]. While hIAPP aggregates are found toxic to insulin-secreting β-cells [8], increasing evidence suggests that small oligomers formed during the early stages of hIAPP aggregation are the main cytotoxic species [9,10]. Characterization of these oligomers including the β-rich oligomers *en route* towards hIAPP fibrillization is, therefore, essential for understanding T2D pathogenesis and for the development of therapeutic strategies against amyloid-associated disease.

Experimental studies of monomeric hIAPP in solution suggest that the peptide mainly adopts a random coil structure, with N-terminal residues 8–19 assuming partially α-helical conformations [11–15]. In vitro studies detected the accumulation of helical intermediate states before their conversion into β-sheet rich aggregates [16–18]. Recently, a study with two-dimensional infrared spectroscopy (2D-IR) revealed that the labeled amyloidogenic region ^{23}FGAIL^{27} of full-length hIAPP

* Corresponding authors.
E-mail addresses: pu-chun.ke@monash.edu (P.C. Ke), fding@clemson.edu (F. Ding).

https://doi.org/10.1016/j.bbadis.2018.11.021
Received 30 August 2018; Received in revised form 10 November 2018; Accepted 26 November 2018
Available online 28 November 2018
0925-4439/

first transformed into ordered β-sheet oligomers with at least five β-strands from random coils and then became partially disordered in the fibrils [19]. Using lipid nanodiscs to trap hIAPP intermediates and structural modeling with NMR constraints, Camargo et al. detected a non-helical intermediate state featuring three antiparallel β-sheets with the amyloidogenic ^{23}FGAIL^{27} in the flexible loop [20]. Using electrospray ionization-ion mobility spectrometry-mass spectrometry (ESI-IMS-MS) [21,22], hIAPP oligomers ranging from dimers to hexamers at the early aggregation stages were detected. The dynamic and heterogeneous nature of these intermediate oligomers renders their experimental isolation and direct characterization challenging, especially for hIAPP whose fibrillization is significantly faster than that of Aβ and α-synuclein. Therefore, it is highly challenging to structurally characterize aggregation oligomers at the atomic level [7,23].

Due to high degrees of freedom and long timescales associated with the nucleation of β-rich aggregates towards amyloid fibrils, previous molecular dynamics (MD) studies either focused on the aggregation dynamics of multiple short hIAPP fragments [24–26], or the structures of full-length hIAPP monomers and dimers [27–33]. For example, discrete molecular dynamics (DMD) simulations - a predictive MD approach with enhanced sampling efficiency [34–36] - were used to show that the hIAPP fragments corresponding to the amyloidogenic core sequence of residues 22–28 - hIAPP22–28 - were able to spontaneously self-assemble into large cross-β aggregates via the nucleation of β-rich aggregates among intermediate oligomers [37]. All-atom MD studies of hIAPP monomers and dimers showed that hIAPP could form extended β-hairpin conformations, proposed to be the building blocks of amyloid fibrils [28,29]. Since hIAPP readily forms oligomers up to hexamers as revealed by mass spec experiments [21,22], the structural and dynamic properties of larger hIAPP oligomers, their assembly dynamics, and the conformational changes from experimentally observed helical intermediates to final β-rich aggregates, remain unknown at the atomic and molecular levels.

Recently, toxic β-rich oligomers in the shape of a cylinder or barrel (i.e., β-barrel) have been discovered in the aggregation of an 11-residue fragment from the slow-aggregating heat-shock protein αB-crystalline (^{90}KVKVLGDVIEV^{100}) [38]. Based on experimental characterizations and computational modeling [39], Do et al. found that several C-terminal fragments of Aβ42 with a length of 11 residues might form similar β-barrel oligomers. The formation of β-barrel oligomers by full-length Aβ40/Aβ42 was supported by recent experimental studies [40,41]. Computationally, the formation of β-barrel oligomers was also observed in aggregation simulations of several short peptides, including fragments from β-2 microglobulin (83–89) [42] and Aβ(16–22) [43,44]. Moreover, systematic DMD simulations of seven short peptides derived from hIAPP, Aβ and α-synuclein suggested that β-barrel oligomers might be common intermediates for amyloid peptides assembling into the cross-β like aggregates, but not for the others that formed polymorphic β-rich aggregates [45]. These well-structured β-barrel oligomers, capable of interfacing across the membrane bilayer and thus compatible with the “amyloid-pore” hypothesis of amyloid toxicity, [46–48] have been proposed as the toxic oligomer species in amyloid aggregation. However, unlike short amyloid peptides, which readily adopt single β-strands to form closed β-sheets as β-barrels [43–45], full-length hIAPP features greater conformational flexibility. It is unclear whether full-length hIAPP could form such β-barrel oligomers, how the β-rich oligomers would be nucleated from the helical intermediates as detected by experiments [16–18], and the relevance of previously observed β-hairpin conformations in hIAPP monomer and dimer simulations [27–32] to the nucleation process.

In this study, biophysical characterizations of early hIAPP aggregation with transmission electron microscopy (TEM) and Fourier transform infrared (FTIR) spectroscopy confirmed the accumulation of α-helical intermediate and the formation of round-shaped aggregations before the rapid formation of amyloid fibrils [16–18]. We further applied atomistic DMD simulations with implicit solvent to investigate the structures and dynamics of these early aggregates of hIAPP. As oligomeric species up to hexamers were detected in recent ESI-IMS-MS studies of hIAPP oligomerization and aggregation [21,22], we simulated multiple molecular systems with the number of hIAPP peptides ranging from one to six. Replica exchange MD (REMD) or DMD simulations (REMD) [35,49], where a generalized ensemble of a molecular system is obtained by performing simulations at a wide range of temperatures with periodic exchanges according to the Metropolis criterion, have been widely used to efficiently explore the free-energy landscape. However, the extrapolation of direct information on kinetics and conformational transitions is challenging for replica exchange simulations. Hence, to directly capture the rare nucleation events towards β-rich aggregates during the early aggregation of hIAPP, we performed a large number (~50) of independent constant-temperature simulations (at 300 K) with relatively long simulation times (~0.5 μs each), an enhance sampling approach similar to the worldwide distributed computing for protein folding [50].

Our large-scale DMD simulation results revealed that the formation of hIAPP aggregates from monomers to hexamers was dynamic, with frequent inter-exchanges between different species. On average, these oligomers contained more helical conformations than β-sheets in agreement with ensemble experimental observations of helical intermediates [16–18], while the average β-sheet content increased with increasing oligomer size. Importantly, with a large number of independent simulations we were able to observe the formation of β-rich aggregates – expected to be rare nucleation events – in ~4–6% trajectories, especially for pentamers and hexamers. These structures were mostly composed of either intra-chain β-hairpins (between strands of 8–16 and 25–33) and inter-chain β-sheets among the C-terminal strands, consistent with a previous hypothesis that the β-hairpin structure was the amyloidogenic precursor of hIAPP [28]. Most importantly, β-barrel like aggregates comprised of four or five peptides were also observed. To the best of our knowledge, this is the first report of β-barrel oligomers as the aggregation intermediates of full-length IAPP, enabled by the efficient DMD algorithm with a simple large-scale simulation protocol. Furthermore, potentials of mean force (PMF) analysis revealed high free-energy barriers towards β-rich oligomers, supporting the nucleated conformational changes of oligomers during amyloid aggregation of hIAPP [19]. Among these β-rich oligomers, β-barrel oligomers with well-defined structures could serve as a novel therapeutic target for T2D.

2. Results and discussion

2.1. Experimental characterization of hIAPP aggregation

The aggregation of hIAPP from 0 to 24 h was monitored with TEM and FTIR (Fig. 1). Formation of small oligomeric species with diameters smaller than 10 nm (Fig. 1b) was observed by TEM after 30 min incubation of freshly dissolved hIAPP (Fig. 1a). The presence of oligomers and protofibrils (Fig. 1c) gradually decreased with the passage of time, until mature and rigid amyloid fibrils were detected after 24 h (Fig. 1d). Following the second-order derivative multi-peak fitting protocol for protein secondary structure analysis with FTIR spectra [51], evolution of secondary structure contents was obtained for hIAPP aggregates at the same time of TEM imaging (Fig. 1e–h) [51]. The accumulation of helical conformations (1656 ± 2 cm^{-1}) coincided with the appearance of small oligomers at 30 min. The conversion from unordered (peaks around 1648 ± 2 cm^{-1}) and helix (1656 ± 2 cm^{-1}) to β-sheet (ranged between 1624 and 1642 cm^{-1}) followed the increase of amyloid fibrils. We note that this structural conversation could be observed directly from the FTIR spectra without multi-peak fitting because of non-overlapping spectral peaks of β-sheets from those of unordered coils and helices. Hence, our biophysical characterizations of hIAPP aggregations confirmed previous observation of the early accumulation of small oligomers with helical conformation. Next, we applied DMD

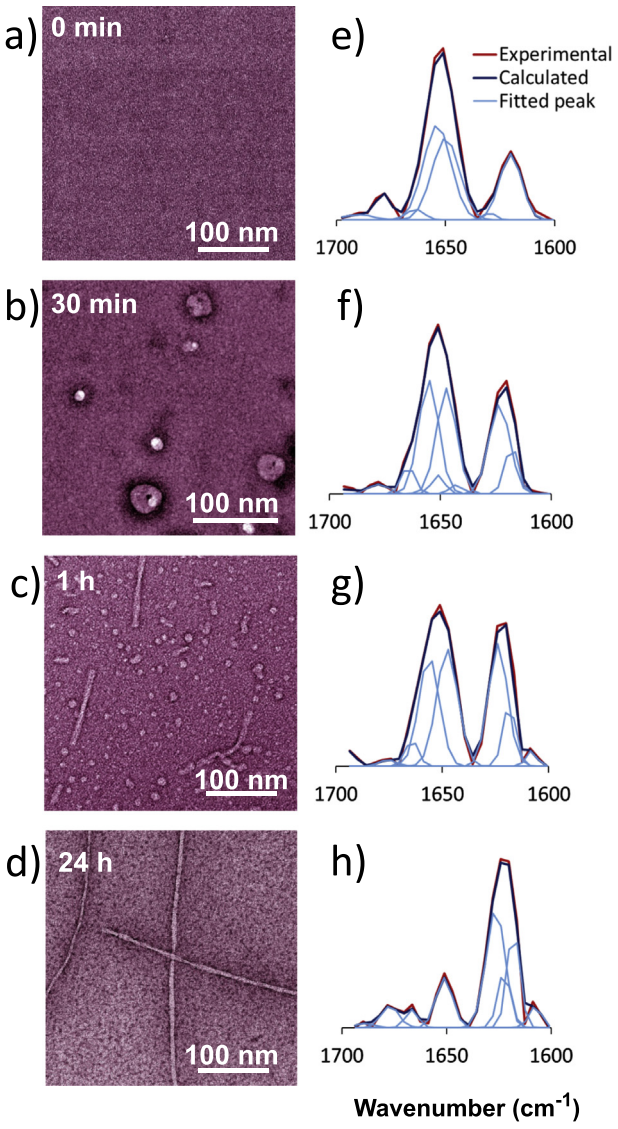

Fig. 1. Experimental studies of hIAPP morphological and structural changes in fibrillization. (a-d) Transmission electron microscopy (TEM) study confirming evolving morphologies of hIAPP from (a) monomeric (not resolvable at circa 1 nm) to (b) oligomeric, (c) oligomeric and protofibrillar and (d) amyloid fibrillar structures. (e-h) Second-order derivative peak fitting of Fourier transform infrared (FTIR) spectra of hIAPP aged 0 min to 24 h, displaying rapid transitions from unordered (peak at $1648 \pm 2\,cm^{-1}$) and helix ($1656 \pm 2\,cm^{-1}$) to β-sheet (ranged between 1624 and $1642\,cm^{-1}$) rich secondary structures.

simulations to uncover the structure and conformational dynamics of these early hIAPP aggregates.

2.2. DMD simulation systems for hIAPP early aggregation

For each of the six molecular systems with one to six peptides, 50 independent simulations were performed starting with randomly generated inter-molecular distances and orientations as well as velocities. The same peptide concentration (~6 mM) was maintained for different systems. The starting conformations of hIAPP were also randomly selected from a conformational ensemble of monomer simulations (Methods). Each independent simulation with more than one peptide lasted ~0.5 μs to ensure sufficient sampling of the diffusion-related assembly process, while the simulation time of each independent monomer simulation was ~0.2 μs. With the large number of

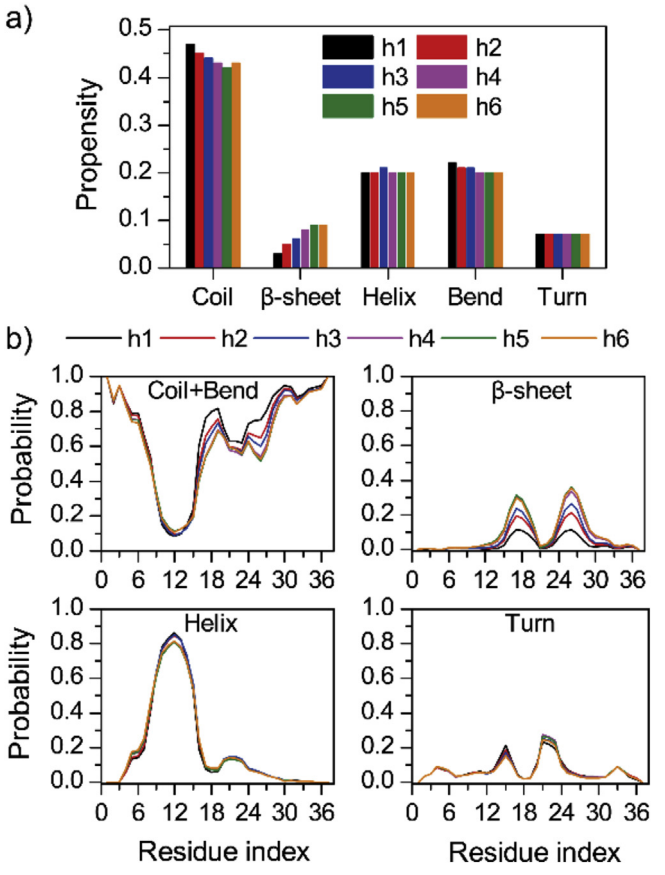

Fig. 2. Secondary structure analysis. (a) Averaged content of secondary structures including coils, β-sheets, helices, bends and turns. (b) Probability of each residue adopting different secondary structures, where coils and bends were combined together as they were not stabilized by hydrogen bonds. The averaging was done over all independent simulations excluding the first 100 ns.

independent simulations, we evaluated the average properties of oligomer distributions and their corresponding secondary and tertiary structural properties, and explored potential conformational transitions towards β-rich oligomers.

2.3. IAPP oligomers had higher content of α-helices than β-sheets on average

We first examined the secondary structures of hIAPP peptides in each of the six simulated molecular systems (Fig. 2), where the first 100 ns simulations of each independent simulation trajectory were discarded to avoid potential biases of starting configurations. On average, hIAPP peptides mainly adopted random coil, helix and bend structures (Fig. 2a). The probabilities of forming β-sheets were low in all simulations (< 0.1), but we did observe an increase in β-sheet content from ~0.03 in the monomer simulations to ~0.09 in the hexamer simulations, accompanying decreases of coil and bend content. With increasing system size the overall helical content remained constant. Analysis of secondary structure propensities per residue (Fig. 2b) indicates that residues around A8-F15 displayed high propensities to form helixes in both monomers and higher order oligomers (~0.4–0.8). The weakly populated β-sheet structures were mainly formed by residues around L16-S20 and G24-S28. This result was consistent with a recent 2D-IR study labeling residues L12A13 and L16 V17 in the early stage of hIAPP aggregation [52], where residues L12A13 were helical but residues L16 V17 were not. The near identical β-sheet propensities per residue around residues 21–23, which showed relatively high propensity to adopt turn conformations (Fig. 2b), are consistent with a β-

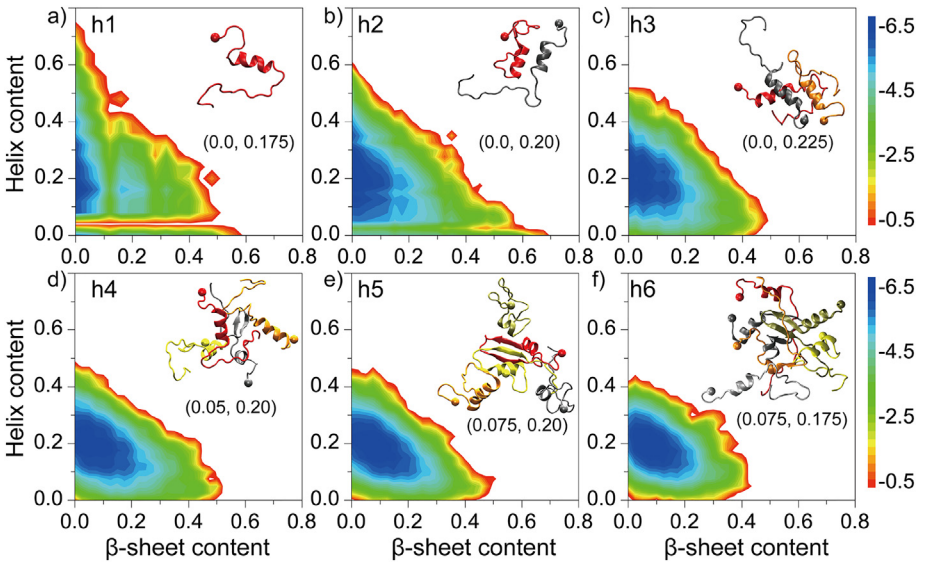

Fig. 3. Potential of mean force (PMF) as a function of helix and sheet contents. The analysis was done for each of the simulated molecular systems, with the number of peptides increasing from one to six (a-f, respectively). Snapshot structures in the insets with helix and β-sheet contents corresponding to the deepest basins were randomly selected from their respective simulations.

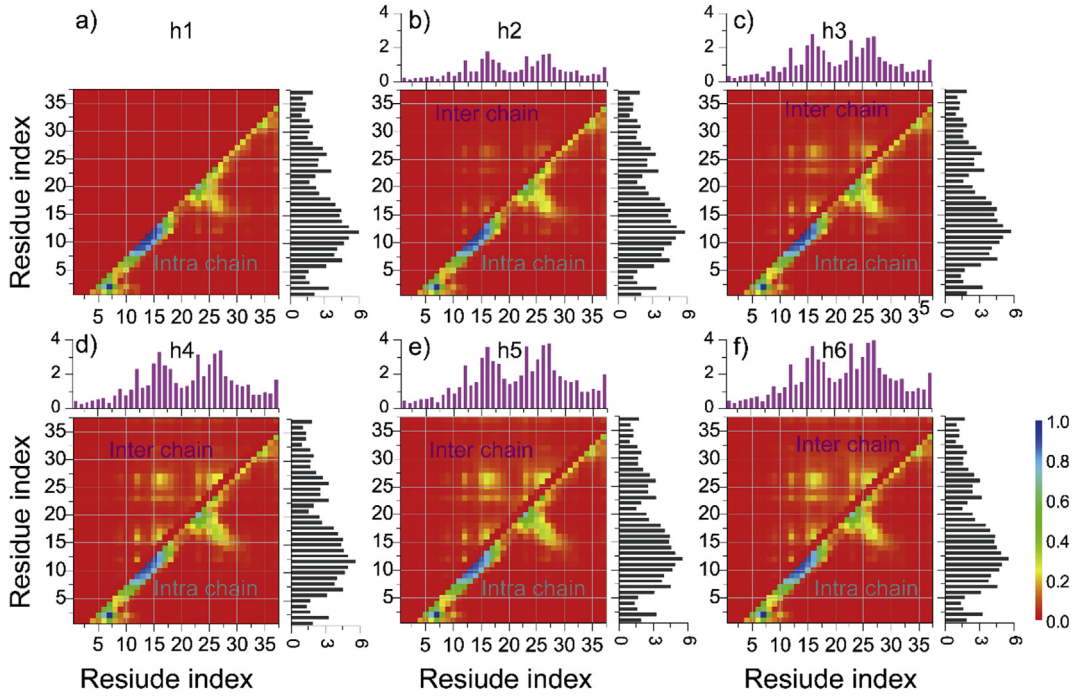

Fig. 4. Analysis of inter-residue interactions. For each of the molecular systems from one to six peptides (a-f), the intra-chain (upper diagonal) and inter-chain (lower diagonal) residue-wise contact frequencies were obtained by averaging over all independent simulations. The total number of intra-chain (black histograms to the right) and inter-chain (purple histograms on the top) contacts per residue was obtained by integrating the corresponding pair-wise contact frequency map.

hairpin structure in the region of residues 16–28.

To better understand the most probable conformation of hIAPPs in each of simulated systems, we computed the potential of mean force (PMF; i.e., the effective free energy) as a function of both β-sheet and α-helix content for each snapshot structure, derived from all independent simulation trajectories (excluding the first 100 ns). As shown in Fig. 3, only one deep free energy basin was observed for all systems. The most populated conformational states corresponding to the free energy basin were α-helices, with their content varying from 0.1 to 0.3. The upper bound of β-sheet content in these basins increased from ~0.05 to ~0.2, with the number of peptides increasing from one to six. As illustrated by typical snapshots, randomly selected with β-sheet and helical content equal to the basin centers (see insets in Fig. 3), these helical-rich oligomers observed in DMD simulations are consistent with previous experimental observations of the accumulation of helical aggregation intermediates [16–18].

We further analyzed the number of residues per chain adopting the β-sheet conformation inside oligomeric aggregates (stabilized by either intra- or inter-chain hydrogen bonds). In addition, via secondary structure analysis of each chain taken out of the context of other peptides, we also estimated the number of β-sheet residues per chain that were stabilized only by intra-chain hydrogen bonds to evaluate the β-hairpin conformation. Despite low-average β-sheet content for all systems, a proportion of peptides with high β-sheet content were consistently present (up to 20–28 out of the total 37 residues, as shown in Fig. S1a). The probability to observe long β-strands and β-hairpins increased with increasing system size. The probability distribution for the number of intra-chain hydrogen bonds was very similar for all systems,

though the average number of inter-chain hydrogen bonds per chain (usually up to 8) displayed a weak increase with increasing system size (Fig. S1b). To characterize the structural properties of these rare β-rich peptides, we also calculated the β-sheet and α-helix propensities per residue for all peptides having a given number of β-sheet residues in oligomeric aggregates (Fig. S2). Residues around A8-F15 displayed a high helical propensity when the total number of β-sheet residues was < 13, where residues 16–20 and 24–28 formed these β-sheets. Peptides with long β-sheets or β-hairpins (e.g., > 15 β-sheet residues) were formed by the conformational conversion of helices in A8-F15 to β-sheet conformations in the N-terminus, as well as a β-sheet growth in the C-terminus.

2.4. Driving forces for hIAPP self-association and oligomerization

To characterize inter-molecular interactions important for hIAPP self-assembly, we computed the intra- and inter-chain contact probabilities between all residue pairs, shown as the contact frequency maps between all atoms (Fig. 4) or between main-chain atoms (Fig. S3). The high intra-chain contact frequencies along the diagonal around residues A8-F15 (~0.8–1.0) were consistent with a high helical propensity in this region. Relatively weaker inter-chain interactions between residues L16-S20 and G24-S28 (probability of ~0.3) with a contact pattern perpendicular to the diagonal were consistent with the formation of a β-hairpin like structure. The total number of intra-chain contacts for each residue, determined by integrating the intra-chain contact frequency map, remained largely the same from monomer to hexamer simulations, though the β-hairpin length increased visibly as the system size increased above three peptides.

The inter-chain interactions were mainly among the sequence stretches of L12-H18 and N22-S28, and their contract frequency patterns revealed that the two subsequences could either self- or cross-associate with each other. This result is consistent with a prior systematic experimental binding assay between full-length IAPP and 10-residue fragments sliding along the sequence, showing that hIAPP12–18 and hIAPP22–28 were the "hot-spot" regions for hIAPP aggregation [53], as well as with a recent hIAPP dimer aggregation study using all-atom REMD simulations with explicit solvent [33]. The segment of ^{23}FGAIL^{27} displayed high contact frequencies with both ^{14}NFLV^{18} and ^{23}FGAIL^{27} segments between main-chain atoms (Fig. S3), indicating that ^{23}FGAIL^{27} could associate into β-sheet structures with both the ^{14}NFLV^{18} and ^{23}FGAIL^{27} segments. The average number of inter-chain contact for each residue increased with increasing system size from dimers to pentamers, and subsequently became saturated. The average number of inter-chain contacts for residues L12, F15, L16, V17, H18, F23, G24, A25, I26, L27, S28 were significantly larger than for the remainder of the sequence, consistent with experimental findings that hIAPP8–20 [54] is a secondary amyloidogenic fragment, in addition to the commonly accepted amyloidogenic core of hIAPP20–29 [55], and in agreement with a mutagenesis study where single mutations of L16Q and I26D inhibited hIAPP aggregation [56]. These results suggest that hydrophobic and aromatic interactions play important roles in the self-association and oligomerization of hIAPP.

2.5. The nucleation of β-sheet rich oligomers and observation of β-barrel oligomers

To assess whether the formation of β-rich structures was heterogeneous, despite no significant shift in average β-sheet content observed with increasing number of peptides in simulations (Fig. 2), we computed the average number of β-sheet and helical residues per chain in the last 400 ns of each independent simulation (Fig. 5), indexed according to the decreasing average number of β-sheet residues per chain. The helical content showed no dependence on system size and weak heterogeneity across different simulations (Fig. 5a). On the other hand, the average number of β-sheet residues per chain increased with

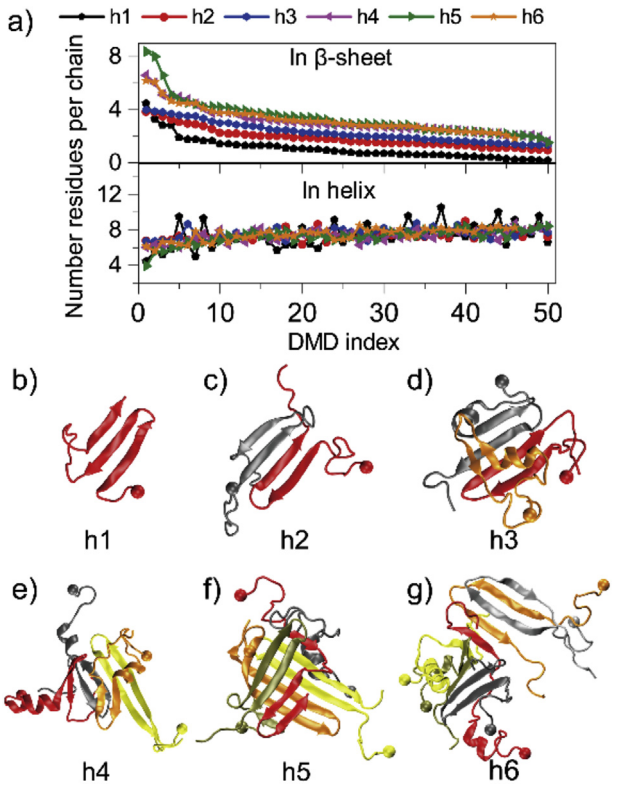

Fig. 5. Heterogeneity in β-sheet formation among independent simulations. (a) The time-averaged number of residues adopting β-sheet (top) or helical (bottom) structures per chain was computed for each independent simulation. Simulation trajectories were sorted according to the averaged β-sheet content from high to low. (b-g) Snapshot structures with high β-sheet contents from the top-ranked trajectories were shown for simulations with one to six peptides.

increasing system size, and featured a high heterogeneity among the simulations – i.e., the first two or three simulations for each system had significantly higher β-sheet content than the rest. Structures with the highest β-sheet content from the top-ranked trajectory for each peptide system were selected in Fig. 5b–g, showing the loss of helices and abundance of β-sheets and β-hairpins. The monomer with the highest β-sheet content in our simulations had three antiparallel β-strands (located around T6-L12, F15-N21 and V32-T36, Figs. 5b & S6) with the amyloidogenic ^{22}NFGAIL^{27} in the loop conformation. This structure is similar to a recently reported non-helical intermediate state of hIAPP, trapped by lipid nanodiscs and computationally reconstructed using NMR constraints [20]. From the pentamer simulations, the most β-abundant oligomer formed the β-barrel like structure (Fig. 5f). β-barrel oligomers have been postulated as the toxic oligomeric species in experimental studies of full-length Aβ40/Aβ42 [40,41] and various other amyloid fragments [38,39,42,43,45]. β-barrel conformations have also been observed previously in silico, but predominantly from simulations of individual short peptide fragments derived from amyloid proteins [39,43,45,57–60]. Systematic DMD simulations investigating the assembly dynamics of the seven short peptides derived from different amyloid proteins suggested that β-barrel oligomers might be the common oligomer intermediates towards the formation of cross-β amyloid fibrils [45]. This observation highlights the ability of full-length hIAPP to also form these potentially toxic β-barrel oligomers.

To characterize hIAPP oligomerization dynamics and conformational transition to β-rich aggregates, we plotted the time evolution of secondary structures for individual residues, in addition to the size of oligomers in which a given peptide participated (along one of the β-sheet abundant trajectories for each peptide system; Fig. 6). In all cases, the oligomerization process reached the "steady state" within 100 ns.

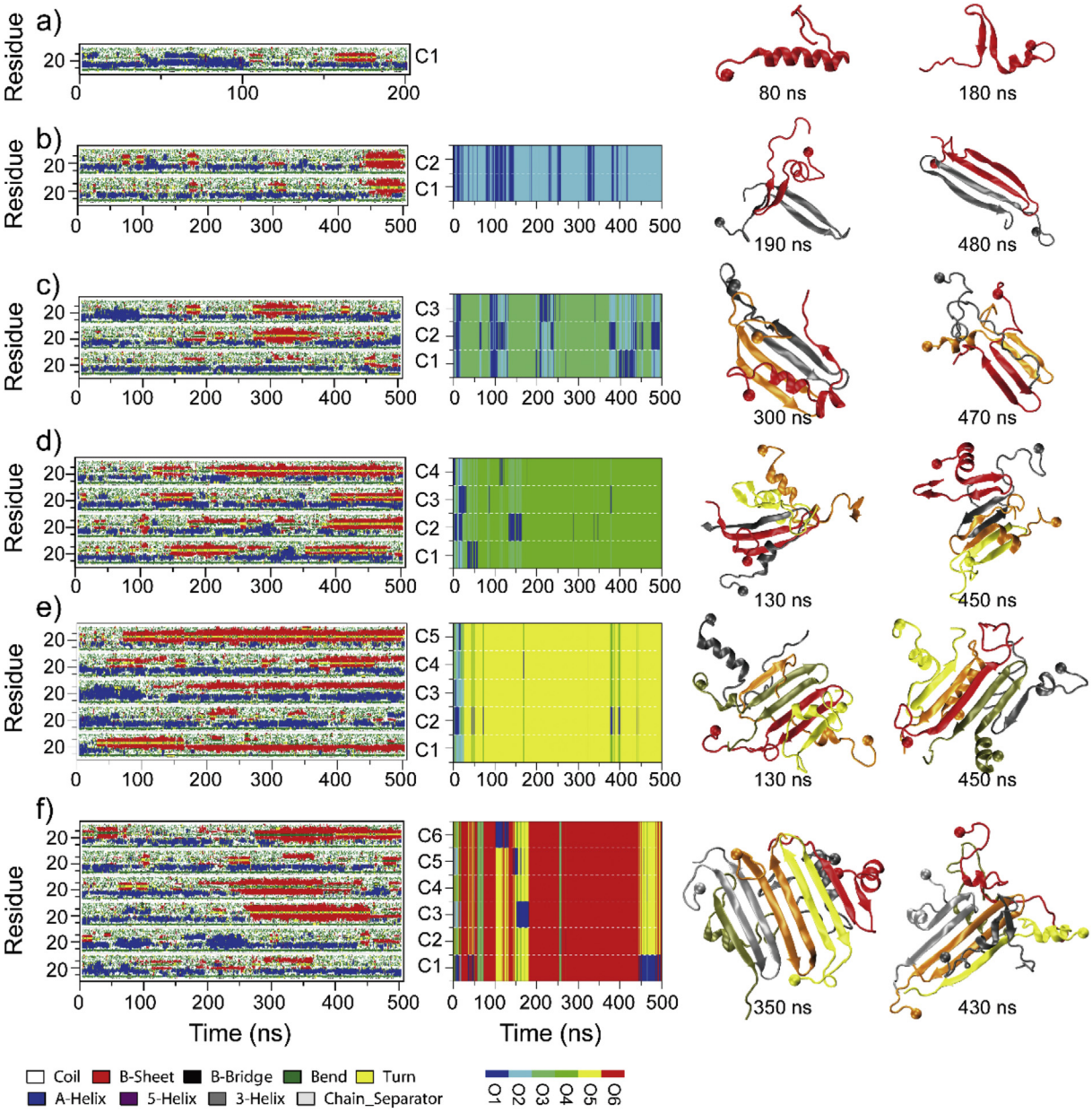

Fig. 6. Oligomerization dynamics and conformational changes. For each of the systems with one to six peptides (a-f), the time evolution of secondary structure per residue (first column) and the oligomer size into which a peptide aggregated (second column) were shown for the most β-sheet rich trajectories. Two snapshots (third and fourth columns, with time stamps blow) were also shown to illustrate the β-sheet rich oligomers.

While the largest oligomers with sizes equal to the total number of peptides in simulations were most populated, these oligomers were usually dynamic; demonstrating, on occasion, dissociation into smaller species. Analysis of the oligomer size distributions for all independent simulations (excluding the initial 100 ns) confirmed the same dynamic oligomerization behavior (Fig. S4). Comparing the emergence of β-sheets (i.e., red pixels in left panels of Fig. 6a–f) with the corresponding oligomeric states (i.e., middle panels of Fig. 6a–f) suggests that the conformational changes to β-sheets usually took place inside oligomers. In most cases, these β-sheets started as intra-chain β-hairpins, featuring the simultaneous appearance of symmetric β-sheets around residues in the turn conformation (i.e., yellow pixels around residues 20 in left panels of Fig. 6a–f). Inside the oligomers, β-hairpins of different chains often grew into large β-sheets by forming inter-chain hydrogen bonds (snapshots in right panels of Fig. 6). These β-sheets were dynamic, with limited duration time (i.e., length of consecutive red pixel regions along the time axes in Fig. 6a–f) during the course of simulations, and the average lifetime increased for oligomers of sizes larger than trimers. The growth of long β-strands from shorter hairpins was often observed (e.g., chains 2&3 at ~280–300 ns in Fig. 6c for a trimer simulation). These long β-hairpin structures (e.g., snapshots in the right panels of Fig. 6a–f) were similar to the β-hairpin reported previously in a hIAPP monomer study combining IMS-MS experiments with implicit-solvent REMD simulations [28]. Mo et al. also observed a similar β-hairpin structure in their hIAPP dimer study, using explicit solvent REMD simulations [33]. In addition, one strand of a hairpin could unfold while the other strand remained in its folded state by interacting with other strands (e.g., chain 1 at ~160 ns in Fig. 5e for a pentamer simulation). Furthermore, peptides could dissociate from oligomers after a loss of β-sheets to favor coil formations (e.g., chain 2 in Fig. 6e around ~375 ns, or chain 1 in Fig. 6f around ~450 ns), suggesting the importance of inter-chain hydrogen bonding in stabilizing these β-rich oligomers.

In order to investigate the dynamics of β-sheet formation, we further analyzed the duration time of stable β-sheet structures in the

simulations of each system. If a peptide had at least five residues in β-sheet conformation for > 1 ns, we treated it as a stable β-sheet conformation and the corresponding duration time was recorded. The average duration of stable β-sheets increased with increasing system size from one to four peptides, and stayed approximately the same for larger systems (Fig. S5a), consistent with the above observation of β-sheet duration from individual trajectories (Fig. 6). As the system size increased, the probability of observing stable β-sheets of all different sizes was enhanced (Fig. S5b). We also calculated the average duration of stable β-sheets as a function of their size for each system (Fig. S5c). As expected, these functions followed an approximately exponential dependence – i.e., longer β-sheets were more stable with longer durations. Interestingly, the slope in the log-linear plot, proportional to the free energy gain for increasing β-sheet size by one residue, also increased with the number of peptides from one to four and became saturated for larger systems. These results suggest that oligomers larger than a trimer allowed the formation of more stable β-sheets, likely by forming larger β-sheets with multiple chains (Fig. 6), so that the boundary effect (i.e., peptides at the edge of a β-sheet with free hydrogen-bond donors and acceptors) was negligible.

2.6. β-barrel oligomers displayed low potential energy, low entropy and high free energy

To better understand aggregation energetics during oligomerization, we computed the PMF as a function of total potential energy and the number of β-sheet residues, using all of the last 400 ns simulation trajectories for the pentamer and hexamer simulations, respectively (Fig. 7a & c). Only one basin was observed for both systems, and hexamers had lower potential energies than pentamers. A general trend for structures with higher β-sheet content having lower potential energies was observed as consequential to the formation of more hydrogen bonds. However, highly β-rich conformations (> 40 β-sheet residues) with low potential energies but high free energies indicate a loss in entropy upon the nucleation of these β-rich oligomers. We noted that the peptide concentrations in our simulations were above the supercritical concentration for a nucleated polymerization process [61,62] where oligomers were more populated than monomers (Fig. S4). Recent experimental studies of Aβ and hIAPP aggregation [19,63] showed persistent aggregation lag-times at high peptide concentrations above the supercritical concentration, suggesting a free energy barrier corresponding to conformational transitions of oligomers. Hence, the observed high free energy barriers associated with conformational transitions towards β-rich oligomers in our simulations support the nucleated conformational conversion of oligomers in amyloid aggregations.

By scanning β-barrel conformations along the simulation trajectories using a hydrogen bond network-based algorithm [44], we also projected the probability of observing β-barrel oligomers within the same two-dimensional coordinates (Fig. 7a & c). We found that β-barrel oligomers were populated in PMF regions with low potential energies and high β-sheet content, corresponding to high free energy values. Representative snapshot structures corresponding to regions in the PMF (Fig. 7b & d) indicate that β-barrel oligomers were mainly composed of either long β-hairpin – with the β-strands located around residues A8-L16 and A25-G33 – or long inter-chain β-strands, formed by residues in the C-terminal while N-terminal residues were mostly helical. The probability of observing β-barrels for each trajectory showed that the nucleation of β-barrel formation was indeed a rare event (Fig. S7). Furthermore, the probability to form β-barrels was enhanced when the number of peptides increased from five to six.

Lipid membranes play important roles in amyloid aggregation and their associated cytotoxicity. Anionic lipid membranes bind positively charged hIAPP to facilitate amyloid aggregation [64,65]. hIAPP fibrillization on the membrane surface accompanies membrane disruption, and residues 1–19 in the N-terminus plays an important role in peptide-membrane interaction [66,67]. The amyloidogenic hIAPP20–29 fragment was found to cause membrane fragmentation but within a narrow concentration range [68]. At higher concentrations, the fibril formation of hIAPP20–29 was enhanced and the membrane fragmentation was significantly inhibited. Other studies pointed to the formation of discrete pores by either helices [64,65] or β-sheets [38,40,41], inducing membrane leakage and cell death [65]. Our observation of β-barrel structures in solution suggested the intrinsic capability of hIAPP to form such a pore-like structures. Recently, Aβ was found to form β-barrel like structures both in the presence [40] and absence [41] of membranes, suggesting that the formation of β-barrel oligomers might be independent of a lipid membrane environment. Further studies are still required to uncover the detailed molecular mechanism of hIAPP oligomerization and fibrillization in the membrane environment in order to fully understand hIAPP amyloid cytotoxicity.

3. Conclusion

We performed all-atom DMD simulations to investigate the oligomerization dynamics and conformational changes during the early aggregation of full-length hIAPP. Six molecular systems with one to six peptides were studied, as oligomeric species up to hexamers were detected in a recent ESI-IMS-MS study of early hIAPP aggregation [21]. To capture the nucleation of β-rich oligomers, we adopted a simple enhanced sampling protocol of performing 50 independent simulations, each of which presented a relatively long simulation time of ~0.5 μs. While high molecular weight oligomers were favored due to high peptide concentration in simulations, the oligomerization process was dynamic, demonstrating frequent inter-conversion between different oligomeric species (Figs. 6, S4). The self-assembly of hIAPP was mainly driven by hydrophobic and aromatic interactions between the primary (residues 22–29) and secondary (residues 15–20) amyloidogenic regions of the hIAPP sequence (Fig. 4). On average, these oligomers had more helical contents than β-sheets (Figs. 2 & 3), consistent with experiments reporting helical intermediates (Fig. 1f) [16–18].

Although the average β-sheet content was relatively low for all simulated systems, with varying numbers of peptides and only weak increases observed with respect to the number of peptides in aggregation simulations, the conversion to β-sheet rich structures was heterogeneous with only a few out of ~50 simulation trajectories featuring high β-sheet contents (Fig. 5). These β-sheet abundant oligomers were mostly composed of either intra-chain β-hairpins (the strand located at residues 8–16 and 25–33) and inter-chain β-sheets among the C-terminal strands, consistent with a prior hypothesis that the β-hairpin structure was the amyloidogenic precursor of hIAPP [28]. Kinetic analysis revealed that long β-sheet structures were more stable in high molecular weight oligomers larger than trimers (Fig. S5, Fig. 6). The estimated aggregation free energy landscape with PMF analysis revealed that β-rich oligomers had lower potential energies but higher free energies due to losses in entropy upon forming well-structured β-sheets (Fig. 7). The observed high free energy barriers associated with conformational transitions towards β-rich oligomers are consistent with the nearly concentration-independent aggregation lag-times at peptide concentrations above the supercritical concentration for both Aβ and hIAPP [19,63]. Hence, our computational results together with prior work [19,63] and our experimental data in this study (Fig. 1) support the nucleated conformational conversion of peptides to oligomers during amyloid aggregation.

Importantly, β-barrels composed of four or five hIAPPs were observed among these β-rich oligomers (Figs. 7, S7). Previous reports of spontaneous formation of β-barrel oligomers were predominantly from simulations of short 7–11 residue fragments derived from amyloid proteins [42] [43–45]. Our study represents the first report of β-barrel oligomers as aggregation intermediate states of full-length hIAPP. These β-barrel oligomers have been postulated to form the membrane-

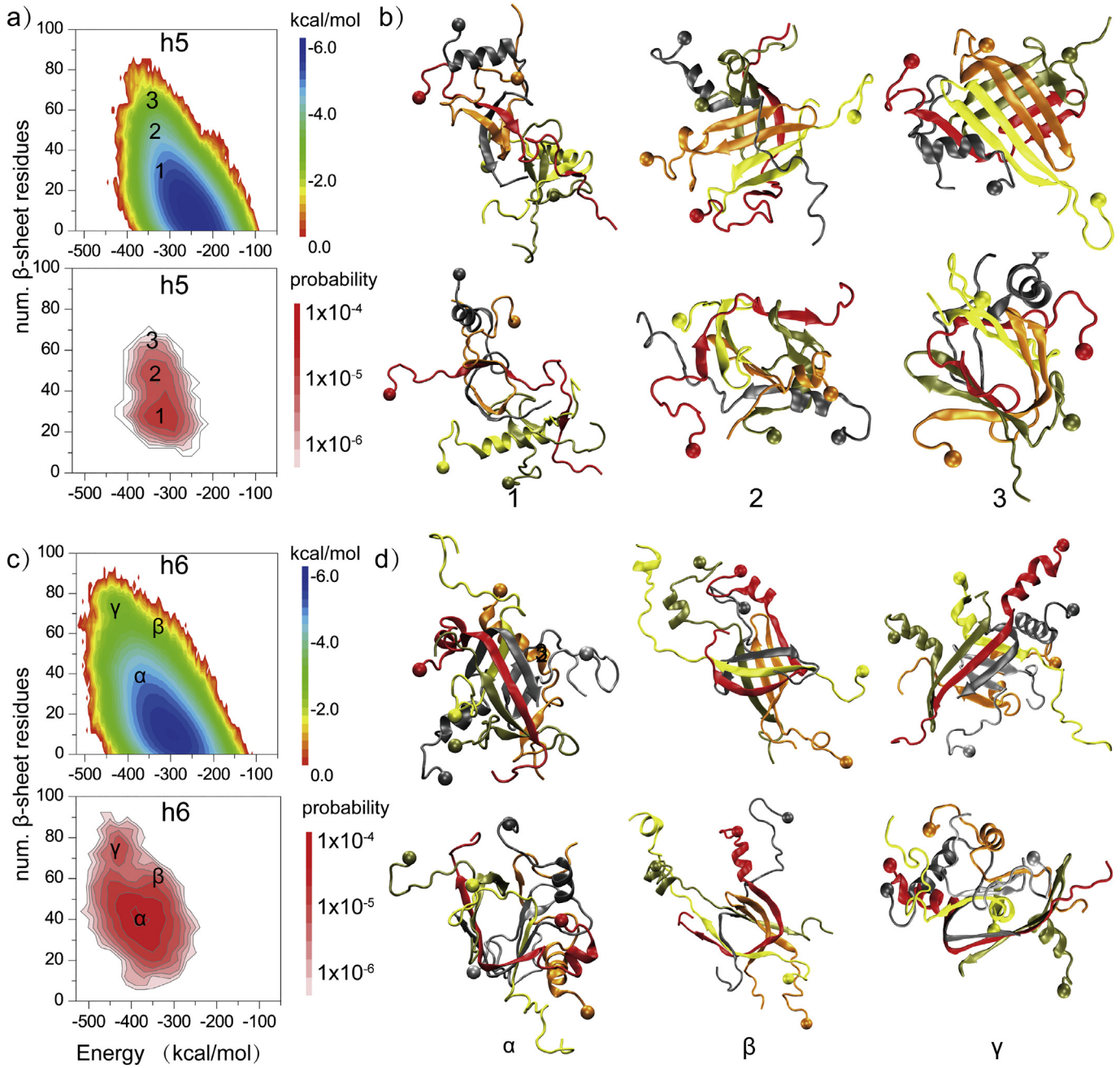

Fig. 7. Aggregation free energy landscapes and population of β-barrel oligomers. The PMF was computed as the function of the potential energy and the total number of residues adopting β-sheet conformation for simulations of five (a) and six (c) peptides, with the population of β-barrels also presented on the same coordinates as the corresponding PMF. To capture the initial aggregation dynamics, the analysis included the whole 500 ns trajectories for all independent simulations with five and six peptides. Representative β-barrel structures in pentamer (b) and hexamer (d) simulations labeled according to their coordinates in the PMFs (1–3, and α-β-γ) were shown in two different views (top and bottom).

associated "amyloid-pores" and play an important role in the pathology of amyloid aggregation; as such, these potentially toxic β-barrel oligomers with well-defined structures could serve as novel therapeutic targets against T2D.

4. Materials and methods

4.1. Transmission electron microscopy

hIAPP aggregation was examined experimentally by transmission electron microscopy (TEM). For this, full length hIAPP (AnaSpec Inc.) was reconstituted overnight in 100% hexafluoro-2-isopropanol (HFIP) to dissolve all preformed aggregates. The solution was then freeze-dried and a stock solution was prepared in Milli-Q water at a concentration of 25 μM. The peptide solution was allowed to aggregate at room temperature up to 24 h and TEM analysis was performed after 0 min, 30 min, 1 h and 24 h of incubation times. For this, 5 μL of peptide-containing solution was pipetted onto a glow discharged (15 s) copper grid (400 mesh; ProSciTech), followed by 1 min of adsorption. Excess sample was then drawn off using filter paper and the grid was washed by Milli-Q water, with the excess drawn off as previously. The grid was stained with a drop of 1% uranyl acetate for 30 s, then the excess stain was drawn off and the grid was air dried. Imaging was performed by a Tecnai G2 F20 transmission electron microscope (FEI, Eindhoven, The

Table 1
Details of molecular systems in DMD simulations, including the number of peptides, corresponding dimensions of the cubic simulation box, number of DMD runs, length of each DMD simulation, and accumulative total simulation times.

Peptide numbers	Dimension (nm)	DMD runs	Simulation time (ns)	Total duration (μs)
1	6.5	50	200	10
2	7.0	50	500	25
3	7.0	50	500	25
4	8.9	50	500	25
5	9.5	50	500	25
6	10.1	46	500	23

Netherlands) operated at a voltage of 200 kV. Images were recorded using a Gatan UltraScan 1000 (2 k × 2 k) CCD camera (Gatan, California, USA) and Gatan Microscopy Suite control software.

4.2. Fourier transform infrared spectroscopy

FTIR spectra were obtained using a Shimadzu IRTracer-100 spectrophotometer. For this, 5 μL aliquots of 25 μM hIAPP after 0 min, 30 min, 1 h and 24 h of incubation were placed on a sample holder, air dried and spectra were acquired between 1000 and 4000 cm^{-1} at 20 °C with resolution of 4 cm^{-1}. A blank spectrum was acquired and subtracted from the sample spectra. Second-order derivative peak fitting of FTIR spectra was performed in Origin.

4.3. Simulation system setup

The sequence of hIAPP is $KCNTATCATQ^{10}$ $RLANFLVHSS^{20}$ $NNFGAILSST^{30}$ $NVGSNTY^{37}$, with the Cys2 and Cys7 forming a disulfide bond. In order to investigate the aggregation dynamics, we studied six different systems with the number of hIAPP peptides increased from one to six. The initial structure of hIAPP for monomer simulations was taken from the protein data bank (PDB ID: 2L86) obtained by an NMR study at physiological pH in a membrane environment [12]. Out of 50 independent monomer simulations (each run lasted 200 ns), we selected 50,000 conformations from the last 100 ns of each trajectory and performed root-mean-square deviation (RMSD)-based cluster analysis [69] with a cutoff of 0.55 nm to select the representative hIAPP monomer structures in solution. The initial structures for simulations with more than one hIAPP peptide were constructed by randomly selecting monomer conformations from the center structures of top ten clusters (representing 24.5% of the monomer ensemble), where the peptides were randomly positioned in the simulation box with any inter-peptide atomic distances larger than 1.5 nm. In all cases, the same peptide concentration of ~6 mM was maintained by adjusting the simulation box sizes. Details of all the simulations are summarized in Table 1.

4.4. DMD simulations

All simulations were performed using the discrete molecular dynamics (DMD) algorithm [34–36]. DMD is a unique type of molecular dynamics algorithm with significantly enhanced sampling efficiency, which has been widely used in studying protein folding [35], aggregation [37], and interactions of small molecules or nanoparticles with proteins and peptides [70–72]. DMD features similar inter-atomic interactions as conventional molecular mechanics force fields, although interaction potentials are modeled by step-wise functions mimicking the continuous potential functions. In the present study, bonded interactions (bonds, bond angles, and dihedrals) were modeled with infinite wells. Non-bonded interactions (i.e., van der Waals, solvation, hydrogen bond, and electrostatic potentials) were represented as a series of discrete energetic steps with increasing distances until reaching zero at the cutoff distance. The van der Waals parameters were based on the CHARMM force field [73], and bonded termed were parameterized based on statistical analysis of protein structures from protein data bank. The solvation effects were implicitly modeled using the EEF1 implicit solvation model developed by Lazaridis and Karplus [74]. The hydrogen bond interactions were depicted by a reaction-like algorithm [75]. Screened electrostatic interactions were modeled by the Debye–Hückel approximation with the Debye length set as 10 Å, corresponding to 100 mM of NaCl under physiological conditions. The units of mass, time, length, and energy were 1 Da, ~50 femtosecond, 1 Å, and 1 kcal/mol, respectively. The temperature of the system was maintained around 300 K using the Anderson's thermostat [76].

4.5. Analysis methods

Secondary structure analyses were performed using the dictionary secondary structure of protein (DSSP) method [77]. A hydrogen bond was considered to be formed if the distance between backbone N and O atoms was ≤ 3.5 Å and the angle of N—H···O ≥ 120°, which was used in prior studies [78,79]. A peptide was considered to have formed a stable β-sheet conformation if it had at least five residues adopting β-sheet structure for > 1 ns during the simulations. Two strands from the same peptide were adjacent, oriented in an antiparallel alignment (the N-terminus of one sheet was adjacent to the C-terminus of the next), and linked by a short loop of two to five amino acids treated as a β-hairpin motif. Inter-chain peptide interactions were analyzed by the residue-residue contact frequency. Here, a pairwise residue contact was defined when the distance between the heavy atoms of two non-sequential residues was < 0.55 nm. If two peptides were connected by at least one inter-chain contact, they were treated to belong to the same oligomer [37]. The two-dimensional potential of mean force, PMF, was constructed using $-K_bTlnP(x, y)$, where K_b is Boltzmann constant, T denotes the temperature of 300 K, and $P(x, y)$ corresponds to the probability of selected reaction ordinates, x and y. If every peptide was connected by two β-sheet neighbors and formed a closed cycle oligomer, this oligomer was treated as a β-barrel structure, similarly to what we defined in a recent study [44].

Conflict of interest

No conflict of interest is declared.

Transparency document

The Transparency document associated with this article can be found, in online version.

Acknowledgement

This work was supported in part by NSF CBET-1553945 (Ding), NIH R35GM119691 (Ding), AFTAM Research Collaboration Award (Davis and Ke), and ARC Project No. CE140100036 (Davis). The content is solely the responsibility of the authors and does not necessarily represent the official views of the NIH and NSF.

Appendix A. Supplementary data

Supplementary data to this article can be found online at https://doi.org/10.1016/j.bbadis.2018.11.021.

References

[1] C.G. Glabe, Common mechanisms of amyloid oligomer pathogenesis in degenerative disease, Neurobiol. Aging 27 (2006) 570–575.
[2] Y. Xiao, B. Ma, D. McElheny, S. Parthasarathy, F. Long, M. Hoshi, R. Nussinov,

Y. Ishii, Abeta(1-42) fibril structure illuminates self-recognition and replication of amyloid in Alzheimer's disease, Nat. Struct. Mol. Biol. 22 (2015) 499–505.
[3] M.D. Tuttle, G. Comellas, A.J. Nieuwkoop, D.J. Covell, D.A. Berthold, K.D. Kloepper, J.M. Courtney, J.K. Kim, A.M. Barclay, A. Kendall, W. Wan, G. Stubbs, C.D. Schwieters, V.M. Lee, J.M. George, C.M. Rienstra, Solid-state NMR structure of a pathogenic fibril of full-length human alpha-synuclein, Nat. Struct. Mol. Biol. 23 (2016) 409–415.
[4] J.J. Wiltzius, S.A. Sievers, M.R. Sawaya, D. Cascio, D. Popov, C. Riekel, D. Eisenberg, Atomic structure of the cross-beta spine of islet amyloid polypeptide (amylin), Protein Sci. 17 (2008) 1467–1474.
[5] S. Luca, W.M. Yau, R. Leapman, R. Tycko, Peptide conformation and supramolecular organization in amylin fibrils: constraints from solid-state NMR, Biochemistry 46 (2007) 13505–13522.
[6] O.S. Makin, L.C. Serpell, Structural characterisation of islet amyloid polypeptide fibrils, J. Mol. Biol. 335 (2004) 1279–1288.
[7] P.C. Ke, M.A. Sani, F. Ding, A. Kakinen, I. Javed, F. Separovic, T.P. Davis, R. Mezzenga, Implications of peptide assemblies in amyloid diseases, Chem. Soc. Rev. 46 (2017) 6492–6531.
[8] S. Zraika, R.L. Hull, C.B. Verchere, A. Clark, K.J. Potter, P.E. Fraser, D.P. Raleigh, S.E. Kahn, Toxic oligomers and islet beta cell death: guilty by association or convicted by circumstantial evidence? Diabetologia 53 (2010) 1046–1056.
[9] T. Gurlo, S. Ryazantsev, C.J. Huang, M.W. Yeh, H.A. Reber, O.J. Hines, T.D. O'Brien, C.G. Glabe, P.C. Butler, Evidence for proteotoxicity in beta cells in type 2 diabetes: toxic islet amyloid polypeptide oligomers form intracellularly in the secretory pathway, Am. J. Pathol. 176 (2010) 861–869.
[10] G.J. Cooper, A.C. Willis, A. Clark, R.C. Turner, R.B. Sim, K.B. Reid, Purification and characterization of a peptide from amyloid-rich pancreases of type 2 diabetic patients, Proc. Natl. Acad. Sci. U. S. A. 84 (1987) 8628–8632.
[11] D.C.R. Camargo, K. Tripsianes, K. Buday, A. Franko, C. Gobl, C. Hartlmuller, R. Sarkar, M. Aichler, G. Mettenleiter, M. Schulz, A. Boddrich, C. Erck, H. Martens, A.K. Walch, T. Madl, E.E. Wanker, M. Conrad, M.H. de Angelis, B. Reif, The redox environment triggers conformational changes and aggregation of hIAPP in type II diabetes, Sci. Rep.-UK (2017) 7.
[12] R.P.R. Nanga, J.R. Brender, S. Vivekanandan, A. Ramamoorthy, Structure and membrane orientation of IAPP in its natively amidated form at physiological pH in a membrane environment, Biochim. Biophys. Acta Biomembr. 1808 (2011) 2337–2342.
[13] S.M. Patil, S.H. Xu, S.R. Sheftic, A.T. Alexandrescu, Dynamic alpha-helix structure of micelle-bound human amylin, J. Biol. Chem. 284 (2009) 11982–11991.
[14] J.A. Williamson, J.P. Loria, A.D. Miranker, Helix stabilization precedes aqueous and bilayer-catalyzed fiber formation in islet amyloid polypeptide, J. Mol. Biol. 393 (2009) 383–396.
[15] M. Apostolidou, S.A. Jayasinghe, R. Langen, Structure of alpha-helical membrane-bound human islet amyloid polypeptide and its implications for membrane-mediated misfolding, J. Biol. Chem. 283 (2008) 17205–17210.
[16] J.A. Williamson, A.D. Miranker, Direct detection of transient alpha-helical states in islet amyloid polypeptide, Protein Sci. 16 (2007) 110–117.
[17] J.A Hebda, A.D. Miranker, The interplay of catalysis and toxicity by amyloid intermediates on lipid bilayers: insights from type II diabetes, Annu. Rev. Biochem. 38 (2009) 125–152, https://doi.org/10.1146/annurev.biophys.050708.133622.
[18] J.J. Wiltzius, S.A. Sievers, M.R. Sawaya, D. Eisenberg, Atomic structures of IAPP (amylin) fusions suggest a mechanism for fibrillation and the role of insulin in the process, Protein Sci. 18 (2009) 1521–1530.
[19] A.L. Serrano, J.P. Lomont, L.H. Tu, D.P. Raleigh, M.T. Zanni, A free energy barrier caused by the refolding of an oligomeric intermediate controls the lag time of amyloid formation by hIAPP, J. Am. Chem. Soc. 139 (2017) 16748–16758.
[20] D.C. Rodriguez Camargo, K.J. Korshavn, A. Jussupow, K. Raltchev, D. Goricanec, M. Fleisch, R. Sarkar, K. Xue, M. Aichler, G. Mettenleiter, A.K. Walch, C. Camilloni, F. Hagn, B. Reif, A. Ramamoorthy, Stabilization and structural analysis of a membrane-associated hIAPP aggregation intermediate, elife 6 (2017).
[21] L.M. Young, P. Cao, D.P. Raleigh, A.E. Ashcroft, S.E. Radford, Ion mobility spectrometry-mass spectrometry defines the oligomeric intermediates in amylin amyloid formation and the mode of action of inhibitors, J. Am. Chem. Soc. 136 (2014) 660–670.
[22] N.F. Dupuis, C. Wu, J.E. Shea, M.T. Bowers, The amyloid formation mechanism in human IAPP: dimers have beta-strand monomer-monomer interfaces, J. Am. Chem. Soc. 133 (2011) 7240–7243.
[23] A.S. Detoma, S. Salamekh, A. Ramamoorthy, M.H. Lim, Misfolded proteins in Alzheimer's disease and type II diabetes, Chem. Soc. Rev. 41 (2012) 608–621.
[24] G. Singh, I. Brovchenko, A. Oleinikova, R. Winter, Demixing transition of the aqueous solution of amyloidogenic peptides: a REMD simulation study, J. Phys. Chem. B 113 (2009) 9863–9870.
[25] W. Xu, P. Jiang, Y. Mu, Conformation preorganization: effects of S20G mutation on the structure of human islet amyloid polypeptide segment, J. Phys. Chem. B 113 (2009) 7308–7314.
[26] P. Jiang, W. Xu, Y. Mu, Amyloidogenesis abolished by proline substitutions but enhanced by lipid binding, PLoS Comput. Biol. 5 (2009) e1000357.
[27] C. Wu, J.E. Shea, Structural similarities and differences between amyloidogenic and non-amyloidogenic islet amyloid polypeptide (IAPP) sequences and implications for the dual physiological and pathological activities of these peptides, PLoS Comput. Biol. 9 (2013) e1003211.
[28] N.F. Dupuis, C. Wu, J.E. Shea, M.T. Bowers, Human islet amyloid polypeptide monomers form ordered beta-hairpins: a possible direct amyloidogenic precursor, J. Am. Chem. Soc. 131 (2009) 18283–18292.
[29] Q. Qiao, G.R. Bowman, X. Huang, Dynamics of an intrinsically disordered protein reveal metastable conformations that potentially seed aggregation, J. Am. Chem. Soc. 135 (2013) 16092–16101.
[30] S. Singh, C.C. Chiu, A.S. Reddy, J.J. de Pablo, Alpha-helix to beta-hairpin transition of human amylin monomer, J. Chem. Phys. 138 (2013) 155101.
[31] R. Laghaei, N. Mousseau, G. Wei, Effect of the disulfide bond on the monomeric structure of human amylin studied by combined Hamiltonian and temperature replica exchange molecular dynamics simulations, J. Phys. Chem. B 114 (2010) 7071–7077.
[32] A.S. Reddy, L. Wang, S. Singh, Y.L. Ling, L. Buchanan, M.T. Zanni, J.L. Skinner, J.J. de Pablo, Stable and metastable states of human amylin in solution, Biophys. J. 99 (2010) 2208–2216.
[33] Y.X. Mo, J.T. Lei, Y.X. Sun, Q.W. Zhang, G.H. Wei, Conformational ensemble of hIAPP dimer: insight into the molecular mechanism by which a green tea extract inhibits hIAPP aggregation, Sci. Rep.-UK 6 (2016).
[34] D. Shirvanyants, F. Ding, D. Tsao, S. Ramachandran, N.V. Dokholyan, Discrete molecular dynamics: an efficient and versatile simulation method for fine protein characterization, J. Phys. Chem. B 116 (2012) 8375–8382.
[35] F. Ding, D. Tsao, H.F. Nie, N.V. Dokholyan, Ab initio folding of proteins with all-atom discrete molecular dynamics, Structure 16 (2008) 1010–1018.
[36] M. Zganec, E. Zerovnik, B. Urbanc, Assembly of Stefin B into polymorphic oligomers probed by discrete molecular dynamics, J. Chem. Theory Comput. 11 (2015) 2355–2366.
[37] Y.X. Sun, B. Wang, X.W. Ge, F. Ding, Distinct oligomerization and fibrillization dynamics of amyloid core sequences of amyloid-beta and islet amyloid polypeptide, Phys. Chem. Chem. Phys. 19 (2017) 28414–28423.
[38] A. Laganowsky, C. Liu, M.R. Sawaya, J.P. Whitelegge, J. Park, M. Zhao, A. Pensalfini, A.B. Soriaga, M. Landau, P.K. Teng, D. Cascio, C. Glabe, D. Eisenberg, Atomic view of a toxic amyloid small oligomer, Science 335 (2012) 1228–1231.
[39] T.D. Do, N.E. Lapointe, R. Nelson, P. Krotee, E.Y. Hayden, B. Ulrich, S. Quan, S.C. Feinstein, D.B. Teplow, D. Eisenberg, J.E. Shea, M.T. Bowers, Amyloid beta-protein C-terminal fragments: formation of cylindrins and beta-barrels, J. Am. Chem. Soc. 138 (2016) 549–557.
[40] M. Serra-Batiste, M. Ninot-Pedrosa, M. Bayoumi, M. Gairi, G. Maglia, N. Carulla, A beta 42 assembles into specific beta-barrel pore-forming oligomers in membrane-mimicking environments, Proc. Natl. Acad. Sci. U. S. A. 113 (2016) 10866–10871.
[41] J. Pan, J. Han, C.H. Borchers, L. Konermann, Structure and dynamics of small soluble Abeta(1-40) oligomers studied by top-down hydrogen exchange mass spectrometry, Biochemistry 51 (2012) 3694–3703.
[42] T. Yoda, Y. Sugita, Y. Okamoto, Comparisons of force fields for proteins by generalized-ensemble simulations, Chem. Phys. Lett. 386 (2004) 460–467.
[43] L.G. Xie, Y. Luo, G.H. Wei, A beta(16–22) Peptides can assemble into ordered beta-barrels and bilayer beta-sheets, while substitution of phenylalanine 19 by tryptophan increases the population of disordered aggregates, J. Phys. Chem. B 117 (2013) 10149–10160.
[44] X. Ge, Y. Sun, F. Ding, Structures and dynamics of beta-barrel oligomer intermediates of amyloid-beta16-22 aggregation, Biochim. Biophys. Acta 1860 (9) (2018) 1687–1697.
[45] Y. Sun, X. Ge, Y. Xing, B. Wang, F. Ding, Beta-barrel oligomers as common intermediates of peptides self-assembling into cross-beta aggregates, Sci. Rep. 8 (2018) 10353.
[46] A. Quist, I. Doudevski, H. Lin, R. Azimova, D. Ng, B. Frangione, B. Kagan, J. Ghiso, R. Lal, Amyloid ion channels: a common structural link for protein-misfolding disease, Proc. Natl. Acad. Sci. U. S. A. 102 (2005) 10427–10432.
[47] M. Kawahara, Y. Kuroda, N. Arispe, E. Rojas, Alzheimer's beta-amyloid, human islet amylin, and prion protein fragment evoke intracellular free calcium elevations by a common mechanism in a hypothalamic GnRH neuronal cell line, J. Biol. Chem. 275 (2000) 14077–14083.
[48] L. Caillon, A.R. Hoffmann, A. Botz, L. Khemtemourian, Molecular structure, membrane interactions, and toxicity of the islet amyloid polypeptide in type 2 diabetes mellitus, J. Diabetes Res. 2016 (2016) 5639875.
[49] Y. Sugita, Y. Okamoto, Replica-exchange molecular dynamics method for protein folding, Chem. Phys. Lett. 314 (1999) 141–151.
[50] B. Zagrovic, E.J. Sorin, V. Pande, Beta-hairpin folding simulations in atomistic detail using an implicit solvent model, J. Mol. Biol. 313 (2001) 151–169.
[51] H. Yang, S. Yang, J. Kong, A. Dong, S. Yu, Obtaining information about protein secondary structures in aqueous solution using Fourier transform IR spectroscopy, Nat. Protoc. 10 (2015) 382–396.
[52] M. Maj, J.P. Lomont, K.L. Rich, A.M. Alperstein, M.T. Zanni, Site-specific detection of protein secondary structure using 2D IR dihedral indexing: a proposed assembly mechanism of oligomeric hIAPP, Chem. Sci. 9 (2018) 463–474.
[53] E. Andreetto, L.M. Yan, M. Tatarek-Nossol, A. Velkova, R. Frank, A. Kapurniotu, Identification of hot regions of the a beta-IAPP interaction Interface as high-affinity binding sites in both cross- and self-association, Angew. Chem. Int. Ed. 49 (2010) 3081–3085.
[54] E.T.A.S. Jaikaran, C.E. Higham, L.C. Serpell, J. Zurdo, M. Gross, A. Clark, P.E. Fraser, Identification of a novel human islet amyloid polypeptide beta-sheet domain and factors influencing fibrillogenesis, J. Mol. Biol. 308 (2001) 515–525.
[55] J. Madine, E. Jack, P.G. Stockley, S.E. Radford, L.C. Serpell, D.A. Middleton, Structural insights into the polymorphism of amyloid-like fibrils formed by region 20-29 of amylin revealed by solid-state NMR and X-ray fiber diffraction, J. Am. Chem. Soc. 130 (2008) 14990–15001.
[56] A. Fox, T. Snollaerts, C. Errecart Casanova, A. Calciano, L.A. Nogaj, D.A. Moffet, Selection for nonamyloidogenic mutants of islet amyloid polypeptide (IAPP) identifies an extended region for amyloidogenicity, Biochemistry 49 (2010) 7783–7789.
[57] Y. Sun, Z. Qian, C. Guo, G. Wei, Amphiphilic peptides A6K and V6K display distinct oligomeric structures and self-assembly dynamics: a combined all-atom and coarse-grained simulation study, Biomacromolecules 16 (2015) 2940–2949.

[58] A. De Simone, P. Derreumaux, Low molecular weight oligomers of amyloid peptides display beta-barrel conformations: a replica exchange molecular dynamics study in explicit solvent, J. Chem. Phys. 132 (2010) 165103.
[59] W. Song, G.H. Wei, N. Mousseau, P. Derreumaux, Self-assembly of the beta 2-microglobulin NHVTLSQ peptide using a coarse-grained protein model reveals beta-barrel species, J. Phys. Chem. B 112 (2008) 4410–4418.
[60] W. Tian, M. Lin, K. Tang, J. Liang, H. Naveed, High-resolution structure prediction of β-barrel membrane proteins, Proc. Natl. Acad. Sci. U. S. A. 115 (7) (2018) 1511–1516, https://doi.org/10.1073/pnas.1716817115.
[61] E.T. Powers, D.L. Powers, The kinetics of nucleated polymerizations at high concentrations: amyloid fibril formation near and above the "supercritical concentration", Biophys. J. 91 (2006) 122–132.
[62] M. Kodaka, Interpretation of concentration-dependence in aggregation kinetics, Biophys. Chem. 109 (2004) 325–332.
[63] J. Lee, E.K. Culyba, E.T. Powers, J.W. Kelly, Amyloid-beta forms fibrils by nucleated conformational conversion of oligomers, Nat. Chem. Biol. 7 (2011) 602–609.
[64] H.R. Patel, A.S. Pithadia, J.R. Brender, C.A. Fierke, A. Ramamoorthy, In search of aggregation pathways of IAPP and other amyloidogenic proteins: finding answers through NMR spectroscopy, J. Phys. Chem. Lett. 5 (2014) 1864–1870.
[65] J.R. Brender, S. Salamekh, A. Ramamoorthy, Membrane disruption and early events in the aggregation of the diabetes related peptide IAPP from a molecular perspective, Acc. Chem. Res. 45 (2012) 454–462.
[66] C. Guo, S. Cote, N. Mousseau, G.H. Wei, Distinct helix propensities and membrane interactions of human and rat IAPP(1-19) monomers in anionic lipid bilayers, J. Phys. Chem. B 119 (2015) 3366–3376.
[67] J.R. Brender, E.L. Lee, M.A. Cavitt, A. Gafni, D.G. Steel, A. Ramamoorthy, Amyloid fiber formation and membrane disruption are separate processes localized in two distinct regions of IAPP, the type-2-diabetes-related peptide, J. Am. Chem. Soc. 130 (2008) 6424–6429.
[68] J.R. Brender, U.H.N. Durr, D. Heyl, M.B. Budarapu, A. Ramamoorthy, Membrane fragmentation by an amyloidogenic fragment of human islet amyloid polypeptide detected by solid-state NMR spectroscopy of membrane nanotubes, Biochim. Biophys. Acta Biomembr. 1768 (2007) 2026–2029.
[69] X. Daura, K. Gademann, B. Jaun, D. Seebach, W.F. van Gunsteren, A.E. Mark, Peptide folding: when simulation meets experiment, Angew. Chem. Int. Ed. 38 (1999) 236–240.
[70] E.N. Gurzov, B. Wang, E.H. Pilkington, P.Y. Chen, A. Kakinen, W.J. Stanley, S.A. Litwak, E.G. Hanssen, T.P. Davis, F. Ding, P.C. Ke, Inhibition of hIAPP amyloid aggregation and pancreatic beta-cell toxicity by OH-terminated PAMAM dendrimer, Small 12 (2016) 1615–1626.
[71] P. Nedumpully-Govindan, E.N. Gurzov, P.Y. Chen, E.H. Pilkington, W.J. Stanley, S.A. Litwak, T.P. Davis, P.C. Ke, F. Ding, Graphene oxide inhibits hIAPP amyloid fibrillation and toxicity in insulin-producing NIT-1 cells, Phys. Chem. Chem. Phys. 18 (2016) 94–100.
[72] P. Nedumpully-Govindan, A. Kakinen, E.H. Pilkington, T.P. Davis, P. Chun Ke, F. Ding, Stabilizing off-pathway oligomers by polyphenol nanoassemblies for IAPP aggregation inhibition, Sci. Rep. 6 (2016) 19463.
[73] B.R. Brooks, R.E. Bruccoleri, B.D. Olafson, D.J. States, S. Swaminathan, M. Karplus, Charmm - a program for macromolecular energy, minimization, and dynamics calculations, J. Comput. Chem. 4 (1983) 187–217.
[74] T. Lazaridis, M. Karplus, Effective energy function for proteins in solution, Proteins 35 (1999) 133–152.
[75] F. Ding, J.M. Borreguero, S.V. Buldyrey, H.E. Stanley, N.V. Dokholyan, Mechanism for the alpha-helix to beta-hairpin transition, Proteins Struct. Funct. Genet. 53 (2003) 220–228.
[76] H.C. Andersen, Molecular-dynamics simulations at constant pressure and-or temperature, J. Chem. Phys. 72 (1980) 2384–2393.
[77] W. Kabsch, C. Sander, Dictionary of protein secondary structure - pattern-recognition of hydrogen-bonded and geometrical features, Biopolymers 22 (1983) 2577–2637.
[78] Y.X. Sun, Z.Y. Qian, C. Guo, G.H. Wei, Amphiphilic peptides A(6)K and V6K display distinct oligomeric structures and self-assembly dynamics: a combined all-atom and coarse-grained simulation study, Biomacromolecules 16 (2015) 2940–2949.
[79] Y. Zou, Y.X. Sun, Y.Z. Zhu, B.Y. Ma, R. Nussinov, Q.W. Zhang, Critical nucleus structure and aggregation mechanism of the C-terminal fragment of copper-zinc superoxide dismutase protein, ACS Chem. Neurosci. 7 (2016) 286–296.